A temperature gradient evaluation method for determining temperature dependent thermal conductivities

OPEN ACCESS
IOP Publishing
Measurement Science and Technology
Meas. Sci. Technol. **32** (2021) 105601 (8pp)
https://doi.org/10.1088/1361-6501/ac0846

A temperature gradient evaluation method for determining temperature dependent thermal conductivities

Sönke Wilhelmy, Anton Zimare, Stephanie Lippmann* and Markus Rettenmayr

Friedrich-Schiller-Universität Jena, Otto Schott Institute of Materials Research, Jena, Germany

E-mail: stephanie.lippmann@uni-jena.de

Received 21 December 2020, revised 28 May 2021
Accepted for publication 4 June 2021
Published 22 June 2021

Abstract

Details of an experimental set-up and an evaluation method for determining temperature dependent thermal conductivities from one-dimensional steady-state temperature distributions are presented. The method is validated by obtaining continuous values for the thermal conductivities of pure Ni in the temperature range between 440 K and 740 K, brass (Cu-30Zn) in the temperature range between 350 K and 650 K and a titanium aluminide (TiAl-TNM) in the temperature range between 400 K and 700 K. The results are in agreement with available literature data. The reported scatter in the literature on conductivities is caused by microstructural or/and compositional differences, which highlights the necessity for swift and accurate experimental determination of thermal properties. For this, the proposed temperature gradient evaluation method is especially suited as it allows the direct determination of thermal properties within large temperature intervals using only a single experimental run. The experimental effort for a comprehensive study of a material is thus drastically reduced as compared to the conventional method of determining thermal conductivity from measured thermal diffusivities and heat capacities. The experimental set-up additionally allows the independent determination of thermal diffusivity as function of temperature. No prior knowledge of any material properties of a given sample is necessary.

Keywords: temperature dependent thermal properties, heat conduction, high-throughput method, Ni, brass, titanium aluminide

(Some figures may appear in colour only in the online journal)

1. Introduction

Thermal properties (thermal conductivity λ, thermal diffusivity α and specific volumetric heat capacity ρC_p) of materials are of practical and scientific interest for numerous applications with exposure to non-homogeneous and/or time-dependent temperature distributions. Without knowledge of these properties as functions of temperature, temperature fields and component performance are predicted inaccurately, and the design of engineering applications is restricted to qualitative amendments [1]. Experimental methods for determining thermal properties are classified as either *transient methods* that evaluate time-dependent signals during heating or cooling of a sample, e.g. transient hot wire method (THW) [2], transient hot strip method (THS) [3, 4], transient and dynamic plane source methods [5–8], laser flash method (LFM) [9], 3 ω method [10] and mirage technique [11, 12], or as *steady-state*

* Author to whom any correspondence should be addressed.

methods evaluating time-independent temperature distributions, such as radial or longitudinal heat flow and guarded hot plate apparatuses [13–16].

It is common practice to determine only either thermal conductivity or diffusivity via one of the above-mentioned methods and to calculate the other property using

$$\lambda = \alpha \cdot \rho C_p, \tag{1}$$

where ρC_p must be known from an auxiliary experimental study or tabulated values. An auxiliary method may introduce further inaccuracies and generally demands additional samples of identical composition and microstructure. Tabulated values might be unavailable or unrepresentative for the material at hand. Further, none of the mentioned methods yields thermal properties directly as function of temperature; instead, data must be interpolated between measurement points that were obtained step-by-step at different temperatures. The required time for this approach can easily exceed 100 h for a single sample [15] as, for the mentioned methods, the sample and experimental set-up must be in thermal equilibrium (or quasi-equilibrium [10]) before the actual measurement. This time is multiplied by each microstructural or compositional variation to be studied of the material. Widely accepted data on thermal properties are thus only available for pure elements and some binary alloys [16–18]. Comprehensive studies on technologically important alloys by the known methods are rare, if not unavailable.

The required time for comprehensive studies may drastically be reduced by determining the thermal properties directly as functions of temperature, thus restricting the experimental effort to a single or very few individual measurements. Recently, an LFM-based method was proposed, allowing temperature dependent calculation of (i.a.) thermal conductivity or specific heat capacity [19]. However, it retains the need for thermal equilibrium before each measurement and for prior knowledge of some of the material's other thermal properties.

In our previous work [20] we introduced a *temperature gradient evaluation method* and an experimental set-up for determining temperature dependent thermal diffusivities without the requirement of thermal equilibrium before the measurement. With this method, thermal diffusivity is measured as function of temperature within temperature intervals of hundreds of K in less than 1 h. The method analyzes temperature profiles in the transient state during heating and determines the thermal diffusivity using an inverse numerical method. However, thermal conductivity is not directly accessible with this method and must still be calculated using equation (1) as well as additional data for the specific volumetric heat capacity of the sample material.

In the present work, we extend our previously introduced experimental set-up [20] to directly determine thermal conductivity as function of temperature by evaluating steady-state temperature distributions. With this extension, thermal conductivity and thermal diffusivity are measured independently using the same sample and experimental set-up. The small sample size drastically accelerates thermal equilibration as compared to other steady-state methods [15]. State-of-the-art transparent insulating materials allow the evaluation of temperature distributions via a state-of-the-art infrared camera with high resolution below 100 µm px^{-1}. The method is validated by comparing measurements on pure Ni, brass (Cu-30Zn) and titanium aluminide (TiAl-TNM) with available reference data from the literature.

2. Materials and methods

2.1. Sample preparation

Rod-shaped samples with diameters of 8 mm and lengths of 60 mm were machined from 99.96% pure Ni (MetalPro, Germany), Cu-30Zn (Wieland, Germany) and TiAl-TNM with a nominal composition of Ti-28.6Al-9.2Nb-2.3Mo-0.026B (GfE Fremat GmbH, AMG Titanium Alloys & Coatings, Germany), respectively. All compositions are given in wt.-%. Ensuring minimal influence of grain boundaries on the material properties, homogenization and grain growth were achieved by annealing the Ni sample at 700 °C for 1 h and the Cu-30Zn sample at 520 °C for 2 h. The TiAl-TNM sample was supplied in a stress-relieved annealed state. Longitudinally, on each cylindrical sample, a 3 mm wide, planar surface was machined.

2.2. Experimental set-up

The samples were mounted in the experimental set-up as shown schematically in figure 1. They were heated at their top ends using middle frequency induction heating ($f = 16$ kHz). Extending our previously introduced set-up [20], the samples were cooled at their lower ends in the streaming mineral oil-based cooling agent Fragoltherm® Q-7 (Fragol AG, Germany). One-dimensional heat flux in axial direction through the sample was ensured by sheathing the sample inside the induction coil with aluminum silicate wool and underneath the coil with silica aerogel, see figure 1. The temperature distribution in the samples was recorded on the machined plane surfaces using a high-resolution infrared (IR) camera (ImageIR® 8380 hp, Infratec GmbH, Germany) that was set up to provide a spatial resolution of 90 µm px^{-1}. The length of the temperature profiles in Ni, Cu-Zn30 and TiAl-TNM were 14.4 mm (160 px), 19.8 mm (220 px) and 18.9 mm (210 px), respectively. In order to minimize the influence of local reflections due surface defects, 17 adjacent temperature profiles were averaged.

Compared to standard bolometer IR cameras, which evaluate temperatures based on the change in resistance of a thermoelectric material, the photon detector IR camera used here exploits the photoelectric effect. This allows the acquisition of temperature profiles in fractions of milliseconds. The manufacturer calibrated the IR camera for the relevant temperature ranges and rates its noise equivalent temperature difference less than 25 mK at 30 °C. For reliable, material independent emissivity, the sample surface was blackened with graphite, ensuring an emissivity of close to unity. Silica aerogel from Airglass Ltd (Sweden) [21] was used to minimize radial heat loss. The material's heat conductivity is given as

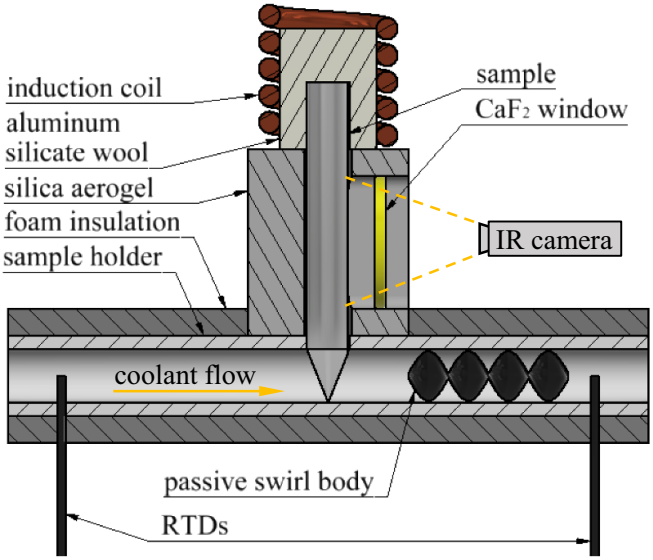

Figure 1. Schematic of the experimental set-up.

0.021 W m^{-1} K^{-1} at 20 °C and 0.2 W m^{-1} K^{-1} at 300 °C [22], the density as 0.13 g cm^{-3} [23] for a representative composition of 92 wt.% $Si0_2$, 5 wt.% C, 1 wt.% H_2, 1 wt.% N_2, and 1 wt.% other components (C and H_2 content may vary depending on the heat treatment) [23]. The pore size of the silica aerogel is ∼10 nm, and Rayleigh scattering is the primary contribution to the attenuation of transmitted [23]. The transmission spectrum of the aerogel follows the properties of silica, but there are two differences, (a) the transmission of silica aerogel already drops significantly starting at 1.4 μm (instead of 2.2 μm for silica) and (b) the aerogel transmits on average 10% in the infrared wavelength range between 3.7 μm and 5 μm. (see silica aerogel transmission spectrum in [24]). The transmission in the infrared range causes heat loss in form of radiation and limits the operating temperature of the current set-up, which is discussed in detail in chapter section 3.3.

Since the aerogel is not fully transparent for IR radiation in the operation range of the IR camera of 2.0–5.7 μm, a slit of 2 mm width for the temperature measurement was cut into the insulation and sealed against air exchange with the environment with a single crystal CaF_2 window (25 × 2 mm^2) and aluminum silicate wool at all remaining gaps. The direction of the temperature gradient was chosen such that the heated air inside the thermal insulation is always colder and denser at the bottom as compared to the top, providing a stable layering and strong reduction of convection.

The cooling agent circulated in a closed loop and its temperature was set to 23 °C in a thermostat bath. The flow rate of the cooling agent $\dot{V}$ was continuously monitored. The temperatures of the cooling agent before and after passing the sample, respectively, were measured using resistance thermal detectors (RTDs), see figure 1. A passive swirl body was inserted into the stream behind the sample and in front of the second RTD to ensure a homogeneous temperature distribution within the cooling agent and thus representative temperature readings from the RTD.

2.3. Determination of thermal conductivity λ*(T)* via gradient evaluation

One-dimensional heat flow in axial direction of the sample is described by Fourier's law as

$$\frac{\dot{Q}}{A} = -\lambda \frac{\partial T}{\partial x}, \tag{2}$$

where $\dot{Q}$ is the heat flow through the cross-section with area A (4.63×10^{-5} m^2) and $\partial T/\partial x$ is the temperature gradient in axial direction. In the steady-state, the heat flow through each cross section of the sample is equal and constant. The temperature dependence of λ implies a spatial dependence of λ in the temperature gradient, leading to deviations from linearity in the temperature profile. Using the IR camera, the temperature distribution in steady-state $T(x)$ is recorded with high resolution, such that the spatial dependence of $\partial T/\partial x$ is obtained from the first derivative of $T(x)$. $\dot{Q}$ is calculated according to

$$\dot{Q} = \dot{V} \cdot \Delta T \cdot \rho C_p, \tag{3}$$

where ΔT is the measured temperature difference between the RTDs, see figure 1, and ρC_p is the specific volumetric heat capacity of the cooling agent, calculated using $\rho(23\,°\mathrm{C}) = 827.9$ kg m^{-3} and $C_p(23\,°\mathrm{C}) = 2.09$ kJ (kg K)$^{-1}$.

With our set-up, typical values of $\dot{V}$ and ΔT are 400–650 ml min^{-1} and up to 2.5 K, respectively. A is determined from the sample dimensions. Equation (2) is thus solved to yield $\lambda(x)$, which is converted into $\lambda(T)$ using $T(x)$. With this approach, a single measurement yields the thermal conductivity directly as function of temperature within the temperature interval defined by $T(x)$.

For recording $T(x)$ in a steady-state, the sample was heated with constant power until the temperature distribution in the sample was stationary. The time needed to reach the steady-state was less than 25 min for all samples. The determination of the temperature gradient $\partial T/\partial x$ is essential for the method. $\partial T/\partial x$ is averaged from several recorded temperature profiles. The measured temperature value at each single pixel is sensitive to disturbances by scratches, dust on the CaF_2 glass and residual roughness of the sample after blackening with graphite, which in combination with the short integration time leads to considerable measurement error for a single temperature measurement. For minimizing this effect, the temperature distribution on the sample surface was recorded over a time span of 60 s with a frame rate of 1 Hz along a total of 17 lines, each parallel to the sample axis and 90 μm wide, resulting in a total of 1 020 temperature profiles. The profiles were filtered using the Savitzky-Golay method [22]. The filter scans the temperature profile of N equidistant pixels. A filter size of 11px was chosen, i.e. at the pixel i with the coordinates (x_i, y_i) the filter window reaches from pixel i-5 to $i + 5$. Within the window, a 1st order polynomial $P_i(x)$ is fitted. The y-value of the filtered ith pixel is then assigned the function value of the fitted polynomial at x_i; it thus has the coordinates $(x_i, P_i(x_i))$. The window of the filter was chosen as small as possible, considering that at the start and the end of the temperature profiles the filter window cannot be defined meaningfully. The filtered profiles

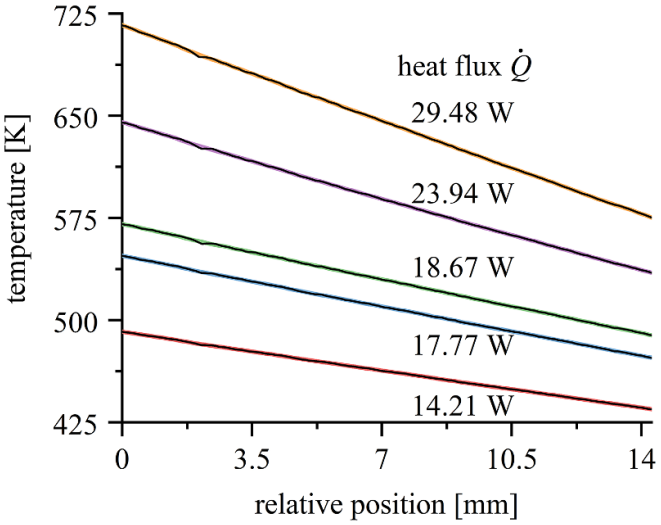

Figure 2. Steady-state temperature profiles measured in Ni, each associated with a heat flux $\dot{Q}$ through the sample that was determined using equation (3), the black lines are non-filtered profiles, the colored profiles are filtered using Savitzky-Golay method [25].

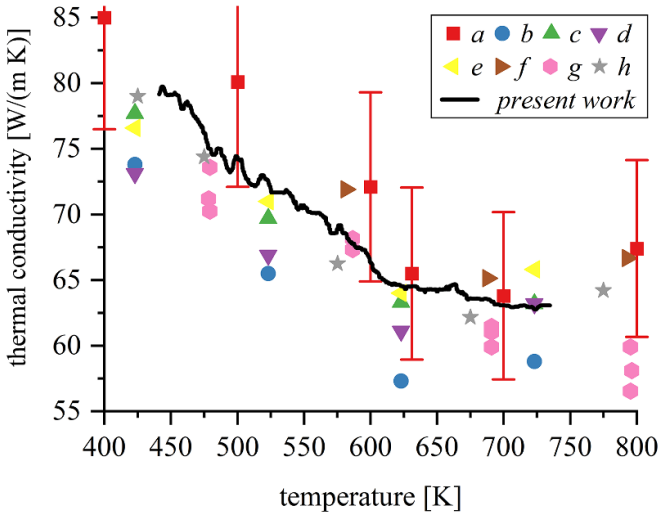

Figure 3. Thermal conductivity of 99.96% pure Ni as measured in the present work using the temperature gradient evaluation method in comparison to *a*: recommended thermal conductivity [16] and experimentally obtained data: *b* sample 1, *c* sample 2, *d* sample 3 and *e* sample 5 from Powell *et al* [26], *f*: Terada *et al* [27], *g*: Endo *et al* [28] and *h*: Jin *et al* [29].

were subsequently averaged to yield $T(x)$ as a single profile with reduced noise.

3. Results and discussion

3.1. Measurements in Ni, Cu-30Zn and TiAl-TNM

Figure 2 presents steady-state temperature profiles that were obtained in Ni by the process described in section 2.3. These colored profiles are not perfectly linear; they are slightly curved owing to the temperature dependence of thermal conductivity. The process for obtaining the temperature dependent thermal conductivities from these profiles is the same for all samples and is described exemplarily using the data for Ni. At each pixel, a value of thermal conductivity is calculated by solving equation (2) using the local temperature gradient. This conductivity value is then assigned to the temperature measured at the respective pixel. Occasionally, the foregoing processing of the temperature profiles does not completely remove the influence of surface defects. These then cause locally confined spikes of the calculated temperature gradient that propagate into the calculation of the thermal conductivity and (locally) lead to implausibly high or low values of conductivity. Such implausible values were replaced by a median of its closely surrounding points. At the boundaries of the measurement range, the replacement by the median can lead to artifacts that are not presented in figures 3–5. The temperature dependent thermal conductivity of Ni is given in figure 3 and is compared with literature values from different sources [16, 26–29]. The slight oscillations between 490 K and 590 K as well as at 670 K in the order of 2 W (m K)$^{-1}$ are remnants of the filtered spikes and could be reduced by increasing the filtering window or by fitting the data with a model equation describing heat conductivity.

The thermal properties of materials vary with temperature, as both lattice vibrations and the mobility of electrons depend on temperature. The thermal conductivity $\lambda(T)$ of Ni (figure 3) distinctly decreases with temperature. The rate of decrease decreases smoothly in the range of about 600 K–620 K, coinciding with the Curie temperature of Ni [30] where the transition from ferromagnetic to paramagnetic behavior occurs. The observed course of the curve is consistent with the reference data [16, 26–29]. These reference data were experimentally obtained by longitudinal heat flow methods for four individual high purity Ni samples (*b, c, d, e*) [26], THS for 99.9% pure Ni (*g*) [28] and thermal diffusivity of >99.9% pure Ni from LFM measurements, converted into thermal conductivity using its specific volumetric heat capacity (*f, h*) [27, 29]. The 'recommended' thermal conductivity for 99.99% pure Ni (*a*) from [16] is based on a critical review of available literature and provides an estimated inaccuracy of up to 10%. The thermal conductivity measured in the present work for 99.96% pure Ni lies well within the margin of error for the recommended data (*a*) from [16] and excellently agrees with the experimental data (*h, c, e*) from [26, 29]. References [16, 26–28] (*a* through *f, h*) all report increasing conductivity at higher temperature, see figure 3. However, our data does not extend to sufficiently high temperatures to include this transition.

Differences in purity, density and microstructure (which is not specified in the literature values) distinctly affect the thermal conductivity of Ni, noticeable as the scatter between curves *b* through *e* that were obtained for individual high purity Ni samples from various suppliers [26]. It is worth noting that [27–29] also report significant deviations between ⩾99.9% pure Ni samples. It is known that microstructural features such as grain size and dislocation density may affect thermal properties, but were not further discussed in [16, 26–29]. Thus, for applications demanding highly accurate

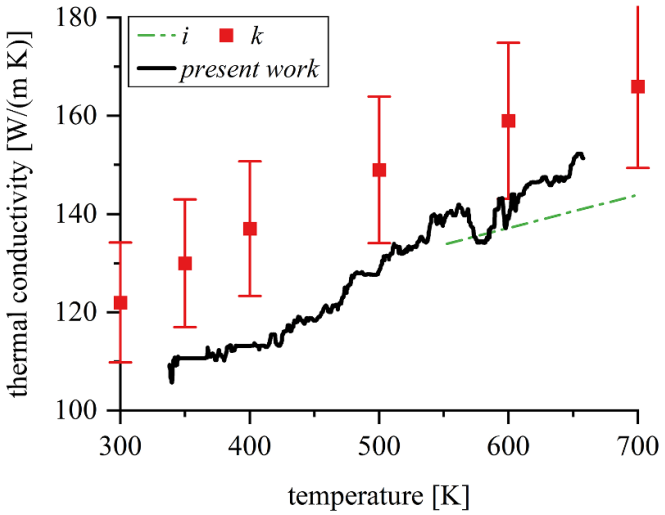

Figure 4. Thermal conductivity of Cu-30Zn as measured in the present work in comparison to *i* (our previous work [20]) and *k* (recommended thermal conductivity with accuracy of ±10% from [18]).

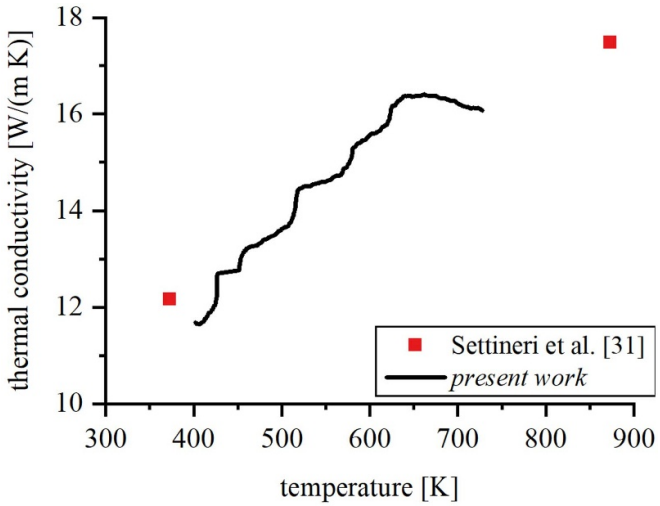

Figure 5. Thermal conductivity of TiAl-TNM as measured in the present work in comparison to two converted thermal diffusivity values from LFM measurements by Settineri *et al* [31].

knowledge of thermal conductivity, reference data should be chosen with care or should be obtained experimentally for a given material state.

Figure 4 presents the temperature dependent thermal conductivity of Cu-30Zn. As expected [18, 20], the values determined by the temperature gradient evaluation method increase with temperature. The thermal conductivity from our previous work [20] was calculated using experimental thermal diffusivity and equation (1); it agrees well with the present data. Differences between the two can arise from the necessary auxiliary ρC_p data used for this calculation. The recommended thermal conductivity for Cu-30Zn [18] is based on a critical review of literature for the Cu-Zn system published from 1908 through 1974. To our best knowledge, no recent experimental studies are available on the temperature dependent thermal conductivity of Cu-30Zn. Compared to the recommended data, our results suggest a somewhat lower thermal conductivity by 10%–18%. The difference between reference and our own values decreases with increasing temperature. This deviation is of similar magnitude as for the different studies on pure Ni presented in figure 3. As discussed previously, we attribute this deviation to microstructural and compositional variations. Recommended data for thermal conductivity cannot fully consider such variations and thus cannot replace experimental measurement of thermal properties for a given material.

Temperature dependent thermal conductivity of TiAl-TNM as obtained by the present temperature gradient evaluation method is displayed in figure 5. An approximately linear increase with temperature is observed. To the best knowledge of the authors, thermal conductivity of TiAl-TNM (within the temperature range presented in figure 5) was previously only reported for two different temperatures by Settineri *et al* [31] using LFM. No estimated accuracy was given for these values and no well-founded estimate of temperature dependence can be established between them. Consistent with the previous discussion, we expect dependencies of thermal conductivity on microstructure and deviations from the nominal composition [31]; nonetheless, the results obtained with the temperature gradient evaluation method agree well with those from [31] and offer additional information about the temperature dependence of thermal conductivity of TiAl-TNM that was previously not reported.

3.2. Uncertainty assessment

In the proposed method, uncertainties arise when (a) calculating the individual thermal conductivity values and (b) assigning calculated thermal conductivities to absolute temperatures. The latter uncertainty is given by the accuracy of temperature measurement via the IR camera. The calibration of the camera is certified and was performed in an authorized lab by the manufacturer. The same graphite as that employed for calibration was used for blackening the sample in the experiments. The certificate specifies 1 K as the accuracy for determining absolute temperatures.

The uncertainty is composed of the uncertainties of the involved measured values, see equations (2) and (3). The absolute value of $\Delta\,(\Delta T)$ is 0.03 K in steady-state. In the extreme case for a material with a very low conductivity of 1 W m^{-1} K^{-1}, the temperature difference in the coolant medium is $\Delta T = 0.3$ K (considering a heat flow of 4.7 W and a temperature gradient of 100 K mm^{-1}), and the relative measurement error could reach a maximum of 10%. The materials used in the present work exhibit thermal conductivities in the range of >12 W m^{-1} K^{-1} and the relative error becomes 2% and smaller.

In the measurement range of the camera, aerogel exhibits some transparency for infrared radiation from 2.0 to 2.7 μm and from 3.7 to 5 μm [24]. For a black body at 750 K (the maximum temperature in this work), a radiation heat loss of ∼10 W cm^{-2} is expected. The aerogel, however, only

transmits a ∼20%. In a worst case scenario, at the highest temperature (750 K) and for the lowest heat conducting sample (9.5 W for TNM), the relative heat loss due to radiation is estimated to be 5% over the upmost 1 mm of the sample length. In reality the heat loss is expected to be distinctly below <5%, since the temperature decreases by 8.75 K per 1 mm length, the aerogel reflects the greater part of the non-transmitted IR radiation, and the sample is not a (perfect) black body.

The flowmeter has two small oval chambers that are alternately filled and emptied. The maximum error is the volume of one chamber, i.e. $\Delta V = 0.55$ ml, and is independent of the measurement time. For a minimum flow rate of $\dot{V} = 300$ ml min^{-1}, the relative error is negligible at 0.2%. The heat capacity of the coolant was taken from the datasheet. A typical error of heat capacities of fluids is 3 to 5%. Overall, for metals and metal alloys the relative error of the heat flow is estimated to be smaller than 5%. Experimentally, the uncertainty of the heat flux was assessed using Cu as an example by independently and simultaneously determining $\dot{Q}$ (i) as described in section 2.3 and (ii) by solving equation (2) for the heat flux, using the recorded temperature profiles and literature values for the thermal conductivity of Cu [16]. The independently obtained values of heat flux matched within ±3%.

For the heat conductivity, in addition to the error of the heat flow, the error of the cross section and the temperature gradient needs to be considered. All samples were machined and their geometries verified with an uncertainty of less than ±1.5% with respect to their cross-sectional areas. The noise equivalent temperature difference for any pixel is given by the manufacturer as 25 mK. However, the method does not only rely on the temperature difference between two adjacent pixels, but processes hundreds of pixels with individual values that follow a common trend. Therefore, random deviations of individual values are compensated, and the already small noise equivalent plays a subordinate role. For the same sample, the same temperature but different steady-state temperature distributions, the experimentally observed deviation for λ(T) is smaller than ±5%.

3.3. Advantages and limitations of method and experimental set-up

The determination of thermal conductivity directly as function of temperature is a unique feature of the temperature gradient evaluation method compared to the established methods. The temperature resolution of this proposed method is set by the difference in temperature between two adjacent pixels of a recorded temperature profile, see figure 2. Owing to the high spatial resolution of the IR camera of 90 µm px^{-1}, each individual temperature profile yields thermal conductivity as quasi-continuous function of temperature within the covered temperature range. The temperature gradient evaluation method thus yields drastically more information per single measurement run than the established methods, such that the experimental effort to comprehensively study thermal conductivity as function of temperature is reduced to a few hours for all samples presented in this work. Hence, for determination of thermal conductivity as function of temperature, the temperature gradient evaluation method is drastically more time-efficient than the established methods. Its results are accurate for materials with thermal conductivities of 12 W (m K)$^{-1}$ and higher, as demonstrated by the present results. Its strengths are most visible if ρC_p data are unavailable, as the method does not rely on such data and allows independent determination of thermal conductivity and thermal diffusivity using the same sample and experimental set-up. The latter evaluates transient states before thermal equilibration [20].

Theoretically, the temperature gradient evaluation method does not impose limitations on maximum or minimum thermal conductivities or temperatures to which the method is applicable. However, such limitations are introduced by the design of the experimental set-up. At present, the set-up is restricted to temperatures between ambient temperature and 750 K, as (a) the aerogel used for insulation is stable up to this temperature and (b) above this temperature the heat loss due to radiation needs to be taken into account. To prevent the transmission between 3.7 µm and 5 µm, opacified silica aerogels are reported to be a promising alternative to exploit higher temperatures [22].

A minimum temperature difference $\Delta T \geqslant 1.0$ K needs to be maintained between the two RTDs to ensure accurate results, see figure 1 and equation (3). Poor electrical conductors that cannot be heated by induction heating can be measured using a susceptor stacked on top of the sample material. With decreasing thermal conductivity, e.g. as in glasses, wood or some ceramics, the time for thermal equilibration increases. For conductivities below 10 W (m K)$^{-1}$, the influence of radial heat loss increases and leads to reduced accuracy. In this case however, the non-contact temperature measurement via the IR camera prevents any additional disturbance of the measured temperature distribution. With contacting alternatives such as thermocouples or RTDs, commonly deployed in other steady-state measurements set-ups [14, 15], such disturbances would have to be accounted for.

4. Conclusion

An advanced experimental set-up for generating one-dimensional temperature profiles using state-of-the-art materials and equipment is presented. For evaluating the temperature gradient, local temperatures were measured contactless and with high resolution (90 µm px^{-1}) allowing the combination of the set-up with an evaluation method for determining the temperature dependent thermal conductivity. The presented method distinguishes itself from other methods as (a) no prior knowledge of the material's other thermal properties (e.g. ρC_p) is necessary, (b) a single measurement is carried out within a time span of minutes and yields information that could otherwise only be obtained by multiple measurements, where each measurement is associated with waiting time for thermal equilibration, and (c) thermal diffusivity

can simultaneously be measured using the same set-up and sample. Future developments pursue on extending the measurement range (temperature and sensitivity) and the process automation.

Data availability statement

The data that support the findings of this study are available upon reasonable request from the authors.

Acknowledgments

The authors gratefully acknowledge financial support of Deutsche Forschungsgemeinschaft (DFG) under grant references LI 2827/1-1 and LI 2827/2-1. An ImageIR® 8380hp by InfraTec GmbH is applied using a high speed MWIR photon detector with the format of (640 × 512) pixels and at full frame rates of 355 Hz. This camera is equipped with a flexible 10 GigE interface and a M = 1.0× microscope lens specially designed to work at object distances of 200 mm. The authors are thankful to GfE Fremat GmbH, AMG Titanium Alloys & Coatings, Brand-Erbisdorf, Germany, for providing the TiAl-TNM master alloys. Furthermore, Sönke Wilhelmy thanks the Friedrich-Schiller-University Jena for the Landesgraduiertenstipendium, a scholarship funded by the state of Thuringia.

ORCID iDs

Sönke Wilhelmy https://orcid.org/0000-0002-6448-7183
Anton Zimare https://orcid.org/0000-0001-9101-8721
Stephanie Lippmann https://orcid.org/0000-0002-8250-4696

References

[1] Moze M, Zupancic M and Golobic I 2020 Investigation of the scatter in reported pool boiling CHF measurements including analysis of heat flux and measurement uncertainty evaluation methodology *Appl. Therm. Eng.* **169** 114938
[2] Vozar L 1996 A computer-controlled apparatus for thermal conductivity measurement by the transient hot wire method *J. Therm. Anal.* **46** 495–505
[3] Gustafsson S E, Karawacki E and Khan M N 1979 Transient hot-strip method for simultaneously measuring thermal conductivity and thermal diffusivity of solids and fluids *J. Phys. D: Appl. Phys.* **12** 1411–21
[4] Gustafsson S E, Karawacki E and Chohan M A 1986 Thermal transport studies of electrically conducting materials using the transient hot-strip technique *J. Phys. D: Appl. Phys.* **19** 727–35
[5] Gustafsson S E 1991 Transient plane source techniques for thermal conductivity and thermal diffusivity measurements of solid materials *Rev. Sci. Instrum.* **62** 797–804
[6] Karawacki E and Suleiman B M 1991 Dynamic plane source technique for simultaneous determination of specific heat, thermal conductivity and thermal diffusivity of metallic samples *Meas. Sci. Technol.* **2** 744–50
[7] Karawacki E, Suleiman B M, Ul-haq I and Nhi B-T 1992 An extension to the dynamic plane source technique for measuring thermal conductivity, thermal diffusivity, and specific heat of dielectric solids *Rev. Sci. Instrum.* **63** 4390–7
[8] Malinarič S and Dieška P 2009 Improvements in the dynamic plane source method *Int. J. Thermophys.* **30** 608–18
[9] Parker W J, Jenkins R J, Butler C P and Abbott G L 1961 Flash method of determining thermal diffusivity, heat capacity, and thermal conductivity *J. Appl. Phys.* **32** 1679–84
[10] Cahill D G 1990 Thermal conductivity measurement from 30 to 750 K: the 3ω method *Rev. Sci. Instrum.* **61** 802–8
[11] Salazar A, Sánchez-Lavega A and Fernández J 1989 Theory of thermal diffusivity determination by the 'mirage' technique in solids *J. Appl. Phys.* **65** 4150–6
[12] Sánchez-Lavega A and Salazar A 1994 Thermal diffusivity measurements in opaque solids by the mirage technique in the temperature range from 300 to 1000 K *J. Appl. Phys.* **76** 1462–8
[13] Fave L, Pouchon M A and Hébert C 2017 A radial heat flow apparatus for thermal conductivity characterisation of cylindrical samples *J. Therm. Anal. Calorim.* **130** 1855–63
[14] Kraemer D and Chen G 2014 A simple differential steady-state method to measure the thermal conductivity of solid bulk materials with high accuracy *Rev. Sci. Instrum.* **85** 025108
[15] Filla B J 1997 A steady-state high-temperature apparatus for measuring thermal conductivity of ceramics *Rev. Sci. Instrum.* **68** 2822–9
[16] Touloukian Y S, Powell R W, Ho C Y and Klemens P G 1970 *Thermal Conductivity–Metallic Elements and Alloys* (New York: IFI/Plenum)
[17] Touloukian Y S, Powell R W, Ho C Y and Nicolaou M C 1973 *Thermal Diffusivity* (New York: IFI/Plenum)
[18] Ho C Y, Ackerman M W, Wu K Y, Oh S G and Havill T N 1978 Thermal conductivity of ten selected binary alloy systems *J. Phys. Chem. Ref. Data* **7** 959–1178
[19] Pavlov T R, Staicu D, Vlahovic L, Konings R J M, Van Uffelen P and Wenman M R 2018 A new method for the characterization of temperature dependent thermo-physical properties *Int. J. Therm. Sci.* **124** 98–109
[20] Zhang Q Y, Lippmann S, Grasemann A, Zhu M F and Rettenmayr M 2016 Determination of temperature dependent thermophysical properties using an inverse method and an infrared line camera *Int. J. Heat Mass Transfer* **96** 242–8
[21] Henning S 1986 Large-scale production of Airglass *Aerogels* (*Springer Proceedings in Physics* vol 6) ed J Fricke (Berlin: Springer) pp 38–41
[22] Ratke L, Fricke J and Reichenauer G 1998 Aerogel for space furnace application, final report ESTEC/Contract no. 12959/NL/MV (3 September)
[23] Holmes N C, Radousky H B, Moss M J, Nellis W J and Henning S 1984 Silica at ultrahigh temperature and expanded volume *Appl. Phys. Lett.* **45** 626–8
[24] Strobach E, Bhatia B, Yang S, Zhao L and Wang E N 2019 High temperature stability of transparent silica aerogels for solar thermal applications *APL Mater.* **7** 081104
[25] Savitzky A and Golay M J E 1964 Smoothing and differentiation of data by simplified least squares procedures *Anal. Chem.* **36** 1627–39
[26] Powell R W, Tye R P and Hickman M J 1965 The thermal conductivity of nickel *Int. J. Heat Mass Transfer* **8** 679–88
[27] Terada Y, Ohkubo K, Mohri T and Suzuki T 1997 Thermal conductivity in nickel solid solutions *J. Appl. Phys.* **81** 2263–8
[28] Endo R, Shima M and Susa M 2010 Thermal-conductivity measurements and predictions for Ni–Cr solid solution alloys *Int. J. Thermophys.* **31** 1991–2003

[29] Jin K, Mu S, An K, Porter W D, Samolyuk G D, Stocks G M and Bei H 2017 Thermophysical properties of Ni-containing single-phase concentrated solid solution alloys *Mater. Des.* **117** 185–92

[30] Wilhelmy S, Zimare A, Zhang Q, Rettenmayr M and Lippmann S 2021 Determining Curie temperature of Ni from temperature dependent thermal properties exploiting temperature gradient evaluation method *Int. Commun. Heat Mass Transfer* accepted (https://doi.org/10.1016/j.icheatmasstransfer.2021.105239)

[31] Settineri L, Priarone P C, Arft M, Lung D and Stoyanov T 2014 An evaluative approach to correlate machinability, microstructures, and material properties of gamma titanium aluminides *CIRP Ann.* **63** 57–60